SYNCRIP, a new player in pri-let-7a processing

YING CHEN,[1,3] JINGRU CHAN,[1,3] WEI CHEN,[1] JIANWEI LI,[1] MENG SUN,[1] GAYATHIRI SATHYAMOORTHY KANNAN,[1] YU-KEUNG MOK,[1] YUREN ADAM YUAN,[1,2,4] and CHACKO JOBICHEN[1]

[1]Department of Biological Sciences and Centre for Bioimaging Sciences, National University of Singapore, Singapore 117543, Singapore
[2]National University of Singapore (Suzhou) Research Institute, Suzhou Industrial Park, Jiangsu 215123, China

ABSTRACT

microRNAs (miRNAs), a class of small and endogenous molecules that control gene expression, are broadly involved in biological processes. Although a number of cofactors that assist or antagonize let-7 miRNA biogenesis are well-established, more auxiliary factors remain to be investigated. Here, we identified SYNCRIP (Synaptotagmin Binding Cytoplasmic RNA Interacting Protein) as a new player for let-7a miRNA. SYNCRIP interacts with pri-let-7a both in vivo and in vitro. Knockdown of SYNCRIP impairs, while overexpression of SYNCRIP promotes, the expression of let-7a miRNA. A broad miRNA profiling analysis revealed that silencing of SYNCRIP regulates the expression of a set of mature miRNAs positively or negatively. In addition, SYNCRIP is associated with microprocessor complex and promotes the processing of pri-let-7a. Strikingly, the terminal loop of pri-let-7a was shown to be the main contributor for its interaction with SYNCRIP. Functional studies demonstrated that the SYNCRIP RRM2–3 domain can promote the processing of pri-let-7a. Structure-based alignment of RRM2–3 with other RNA binding proteins identified the residues likely to participate in protein–RNA interactions. Taken together, these findings suggest the promising role that SYNCRIP plays in miRNA regulation, thus providing insights into the function of SYNCRIP in eukaryotic development.

Keywords: SYNCRIP; miRNA biogenesis; pri-let-7a processing

INTRODUCTION

miRNAs are a class of small, endogenous molecules that post-transcriptionally regulate gene expression according to their sequence complementarity to mRNA, leading to mRNA instability, or translational inhibition (Bartel 2009; Fabian et al. 2010). Therefore, miRNAs are broadly involved in various biological processes, and aberrant expression of miRNAs is closely related to a variety of diseases, cancer initiation, and progression (Croce 2009; Mendell and Olson 2012; Lin and Gregory 2015).

let-7 miRNA, discovered as the first miRNA in human, is a conserved molecule among eukaryotes. A wide range of studies revealed the multiple functions of let-7 miRNA in the regulation of developmental timing and carcinogenesis. In worms, loss-of-function of let-7 miRNA affects cell division, blocks the transition from larval to adult stage, causing lethality (Reinhart et al. 2000). In flies, let-7 controls developmental stage transition similar to what was observed in worms (Bashirullah et al. 2003) and the maturation of neuromuscular junctions (NMJs) (Caygill and Johnston 2008; Sokol et al. 2008). In mammalian cells, let-7 regulates timed development, and also acts as a tumor suppressor.

Transcribed by RNA polymerase II (RNA pol II) (Lee et al. 2004), canonical primary miRNAs (pri-miRNAs) fold back to form a stem–loop structure, which are processed sequentially by Drosha and Dicer in nucleus and cytoplasm, respectively (Hutvagner et al. 2001; Ketting et al. 2001; Lee et al. 2003). In the nucleus, Drosha-mediated cleavage generates ~65 nt, hairpin-structured precursor miRNAs (pre-miRNAs) which are later transported into an the cytoplasm by Exportin 5 in a Ran-GTP-dependent manner (Yi et al. 2003; Bohnsack 2004; Lund et al. 2004). In the cytoplasm, pre-miRNAs are further cropped into an miRNA duplex, and one strand of which, the mature miRNA, is incorporated into RISC (RNA-induced silencing complex). The mature miRNA serves as a guide for Agonaute2 (AGO2) to drive the molecular machinery for RNAi (Kobayashi and Tomari 2016). miRNA biogenesis is an intricate, multistep process where regulation could occur to fine-tune the expression of miRNA in accordance

[3]These authors contributed equally to this work.
[4]Deceased.
Corresponding author: jobichenc@nus.edu.sg
Article is online at http://www.rnajournal.org/cgi/doi/10.1261/rna.072959.119.

with differentiation and development requirements. Up to date, a series of sequence determinants on miRNA precursors are known and a number of protein regulators have been well-recognized that define microprocessor targets and fine-tune miRNA expression level, respectively (Gebert and MacRae 2019; Michlewski and Cáceres 2019). The terminal loop, a unique but conserved feature for miRNA precursors, not only contains determinants to orientate the microprocessor but provides a major landing platform attracting RNA binding proteins (RBPs) to exert regulatory function. Of interest, it was reported earlier that only RRMs are sufficient to induce conformational destabilization of stem–loop structure, which promotes or inhibits nuclear processing (Chen et al. 2016; Kooshapur et al. 2018). In addition to the terminal loop, several regulators recognize specific sequences embedded in the flanking region; for example, QKI5 promotes pri-miR-124 processing by recognizing a distal element away from the stem–loop structure (Wang et al. 2017). For let-7 miRNA, a number of modulators have been identified, such as Lin28 (Heo et al. 2008), hnRNP A1 and KSRP (Michlewski and Caceres 2010), which dock on to its terminal loop and regulate its expression positively or negatively. However, our understanding of post-transcriptional regulation in miRNA biogenesis remains at an early stage and more auxiliary factors await investigation regarding the incredible functions of miRNAs in cellular pathways.

SYNCRIP (also known as hnRNP Q or NSAP1) is an evolutionarily conserved RBP across eukaryotic organisms and participates in several cellular pathways and diseases, especially in neuronal and muscular development. On the RNA side, SYNCRIP has multiple roles in the control of RNA metabolism through recognizing a variety of sequences and regulating pre-mRNA splicing, translation, transport as well as degradation. For example, SYNCRIP modulates alternative splicing of *SMN2* transcript, which may compensate the loss of SMN1 in spinal muscular atrophy patients (Chen et al. 2008). In addition, SYNCRIP specifically recognizes the AUAAUC sequence to regulate the localization of a set of mRNAs, which may further modulate neuronal morphogenesis (Chen et al. 2012). Of particular interest, recently, SYNCRIP was revealed to trigger a vehicle machinery which partitions miRNAs out of cytoplasm to exosome. The molecular principles include wide recognition of mature miRNAs containing hEXO sequence (GGCU/A) and mediation of miRNAs enrichment in exosomes (Santangelo et al. 2016; Hobor et al. 2018).

Although SYNCRIP has been implicated in various aspects of pre-mRNA splicing, RNA localization as well as mRNA translation, its effect on pri-miRNA processing has not been established. Here, we identified that pri-let-7a interacts with SYNCRIP both in vivo and in vitro and this interaction contributes to increased expression of let-7a miRNA. In addition, miRNA microarray results revealed that the regulation controlled by SYNCRIP is not limited to let-7a miRNA; in fact, a subset of miRNAs are regulated by SYNCRIP. The molecular basis underpinning this regulation includes the interaction with DiGeorge Syndrome Critical Region gene 8 (DGCR8) and enhanced microprocessor-mediated processing. Of particular interest, we found that SYNCRIP binds to the terminal loop of let-7a precursors and we identified one of its recognized sequences, UAGAAU, on the apical loop of let-7a precursors. Furthermore, studies on domain function showed that the two tandem RNA recognition motifs (RRMs; RRM2–3) of SYNCRIP harbor the function of the full-length protein to promote pri-let-7a processing. Notably, SYNCRIP is a new regulator in let-7a miRNA biogenesis, which sheds light on SYNCRIP-mediated developmental abnormality.

RESULTS

SYNCRIP binds to pri-let-7a both in vivo and in vitro

Previous work in our laboratory identified a list of potential protein factors for pri-let-7a processing based on an in vivo assay, tRSA-RNA affinity assay (Zheng et al. 2017). SYNCRIP was chosen from the list due to its intensive role in regulation of RNA metabolism. Therefore, we examined interaction between SYNCRIP and pri-let-7a as the first validation step. Repeating the tRSA-pri-let-7a-1 affinity assay (Fig. 1A) showed that SYNCRIP was detected from the bound fraction of pri-let-7a-1 but not from that of the tRSA transcript alone (Fig. 1B). Additionally, an in vitro RNA affinity assay was performed (Fig. 1C) and it was observed that SYNCRIP was efficiently pulled down (Fig. 1D).

We next analyzed the physical interaction of SYNCRIP to pri-let-7a using an RNA immunoprecipitation (RIP) assay, and the primers are shown in Figure 1E. The results showed that SYNCRIP could bind with endogenous pri-let-7a-1 (Fig. 1F,G). To further examine the direct interaction between pri-let-7a-1 and SYNCRIP, an RNA electrophoresis mobility shift assay (RNA-EMSA) was carried out. Migrating bands signifying a SYNCRIP/pri-let-7a-1 complex confirmed the direct interaction of SYNCRIP with pri-let-7a-1 (Fig. 1H). Notably, different sizes of SYNCRIP/pri-let-7a-1 complex formed in a dose-dependent manner with the addition of increasing amounts of recombinant SYNCRIP (rSYNCRIP) protein, suggesting that SYNCRIP may form multimers when incubated with different ratios of RNA. Additionally, we immobilized biotinylated pri-let-7a onto streptavidin BLI sensors to further confirm the interaction and measured the binding affinity with rSYNCRIP. The association and dissociation analysis showed that rSYNCRIP binds to pri-let-7a with high affinity, and yielded a Kd value of 38.2 nM (Supplemental Fig. S1A). By using these approaches, we confirmed that SYNCRIP interacts with pri-let-7a both in vivo and in vitro.

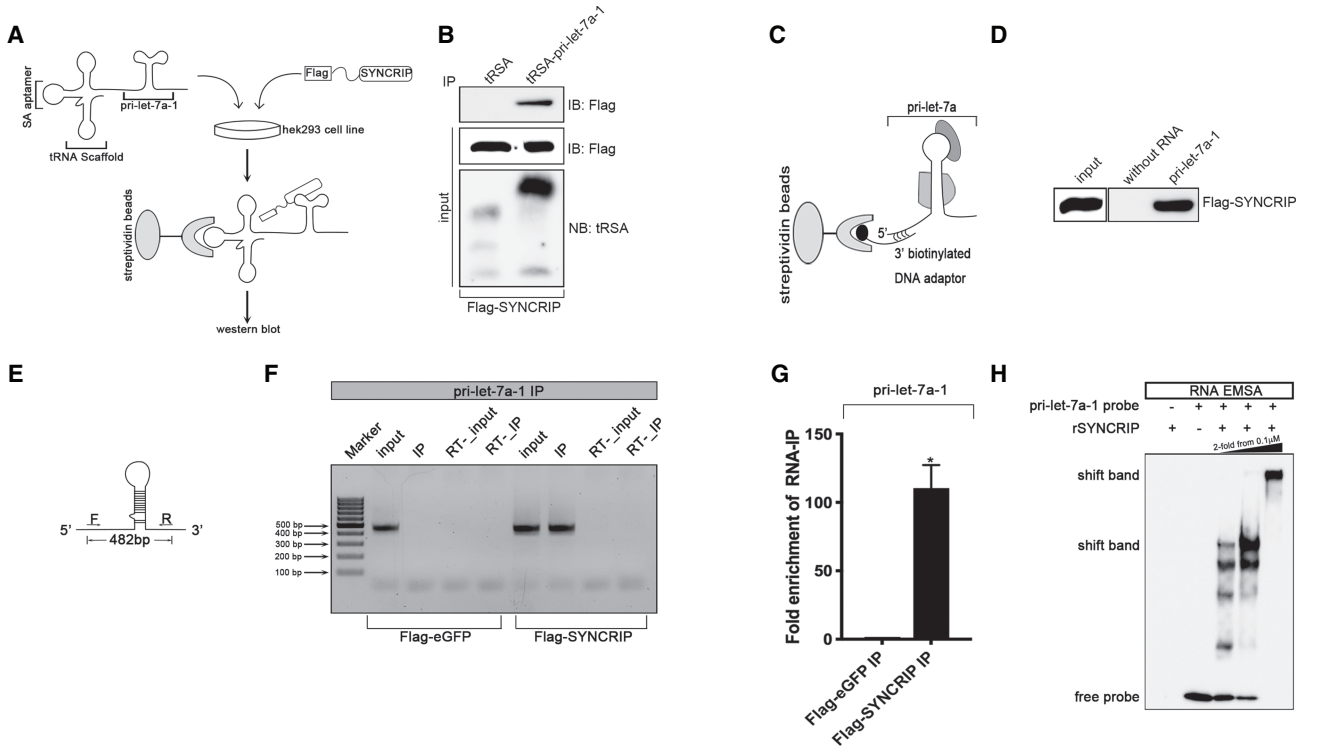

FIGURE 1. SYNCRIP binds to the pri-let-7a-1 both in vivo and in vitro. (*A*) A schematic representation of in vivo tRSA-RNA affinity assay using pri-let-7a-1 in fusion with tRSA tag in HEK293 cells overexpressed with FLAG-tagged SYNCRIP. (*B*) Detection of the presence of FLAG-SYNCRIP in the bound fraction of either tRSA (control) or tRSA-pri-let-7a-1 by in vivo tRSA-affinity assay. The eluate fraction and 5% of protein input were analyzed by immunoblot against FLAG tag. Five percent of RNA input was analyzed by northern blotting using DNA probe against tRSA tag. (*C*) A schematic representation of in vitro RNA affinity assay. Pri-let-7a-1 with short 5′ extension was in vitro transcribed and immobilized with streptavidin-coated Sepharose beads via 3′-biotinylated DNA adaptor, the sequence of which is reverse-complementary to the 5′ extension. (*D*) Pull-down of overexpressed FLAG-tagged SYNCRIP using pri-let-7a-1. The eluate fraction and 5% of protein input were analyzed by immunoblot against FLAG tag. 3′-biotinylated DNA adaptor immobilized on streptavidin-coated Sepharose beads was used as a control. (*E*) A schematic representation of primers used in RNA-IP PCR analysis. (*F*) RIP–PCR analysis of pri-let-7a-1 performed with anti-FLAG beads in HEK293 cells transfected with either flag-eGFP (negative control) or flag-SYNCRIP. (RT) No reverse-transcribed PCR. (*G*) qPCR analysis of pri-let-7a-1 bound with FLAG-SYNCRIP in RIP assay in HEK293 cells. The RIP–qPCR results were shown as fold enrichment compared with input. (*H*) RNA-EMSA assay using biotin-labeled pri-let-7a-1 (0.1 μM). Increasing concentration of purified recombinant his-SYNCRIP was indicated (0.1–0.4 μM).

SYNCRIP regulates the expression of a set of miRNAs

Next, we investigated the biological function of SYNCRIP binding to let-7a primary transcript, to explore whether SYNCRIP/pri-let-7a interaction contributes to miRNA processing in vivo. For loss-of-function analysis, shRNA against SYNCRIP expressed in HEK293 cells and half of SYNCRIP was reduced at mRNA level (Supplemental Fig. S2A). Under this condition, we examined the expression level of primary as well as mature transcripts of let-7a miRNA and observed that knockdown of SYNCRIP has no effect on the expression of pri-let-7a, but it leads to a significant decrease in the expression of mature let-7a (Fig. 2A,B), implying the post-transcriptional regulation by SYNCRIP. We further confirmed the trends using an overexpression assay (Supplemental Fig. S2B). As expected, the expression level of pri-let-7a does not show significant change, while that of let-7a mature miRNA significantly increased, in response to SYNCRIP overexpression (Fig. 2C,D). These findings confirmed that SYNCRIP is required for the expression of endogenous let-7a, and the overexpression of SYNCRIP could promote the generation of let-7a. Extending this finding to other miRNAs, we chose several targets for further verification. A recent study reported that SYNCRIP has specific interaction with certain pre-miRNAs, including pre-let-7a-2, pre-miR-15b, pre-miR-16-1 (Treiber et al. 2017). As pre-let-7a-1 and pre-let-7a-2 both produce let-7a-5p, we selected miR-15b-5p and miR-16-5p for further validation. In addition, miR-26b-5p was randomly picked. We found that knockdown of SYNCRIP causes significant decrease in the expression of miR-16-5p as well as miR-26b-5p (Supplemental Fig. S2C,E), while mild decrease was observed in miR-15b-5p expression (Supplemental Fig. S2D), strongly suggesting that SYNCRIP is capable of regulating miRNAs.

In order to figure out how many miRNAs are regulated by SYNCRIP, we performed miRNA microarray analysis

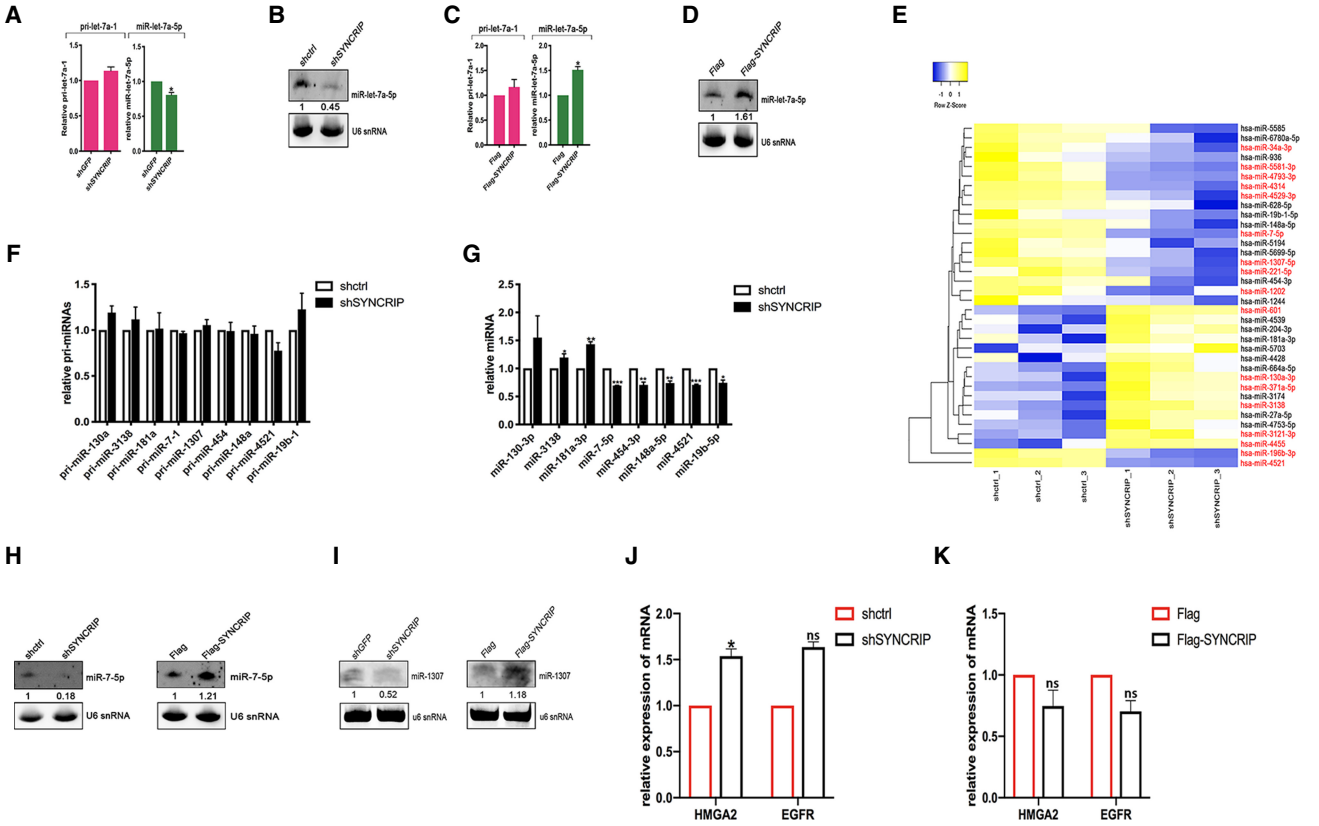

FIGURE 2. SYNCRIP is capable of regulating a set of miRNAs. (*A*,*C*) Real-time PCR analysis of pri-let-7a-1 and let-7a-5p in response to SYNCRIP knockdown (*A*) or overexpression (*C*), respectively. (*B*,*D*) Northern blot analysis of let-7a-5p miRNA in response to SYNCRIP knockdown (*B*) or overexpression (*D*), respectively. (*E*) Microarray expression profile of human miRNAs (fold change >1.5) in SYNCRIP knockdown samples (shSYNCRIP) compared with control sample (shctrl). Those miRNAs with adjusted *P*-value <0.05 were labeled in red. (*F*,*G*) Real-time PCR validation of candidate pri-miRNA (*F*) and mature miRNA (*G*) in SYNCRIP knockdown samples compared with control samples. (*H*,*I*) Northern blot analysis of miR-7-5p (*H*) and miR-1307-5p (*I*) in response to SYNCRIP knockdown (*left* panel) and overexpression (*right* panel). (*J*,*K*) Real-time PCR analysis of the expression of HMGA2 and EGFR, which are the target genes of let-7a-5p miRNA and miR-7-5p, respectively, in response to SYNCRIP knockdown (*J*) or overexpression (*K*). Significance in all real-time PCR analysis was determined by two-tailed *t*-test with (*) $P < 0.05$; (**) $P < 0.01$; (***) $P < 0.001$; ns, non-significant

using SYNCRIP-knockdown samples. Among the 675 human miRNAs that have been analyzed, six miRNAs were significantly (fold change >1.5) up-regulated and 11 miRNAs were significantly down-regulated (Fig. 2E; Supplemental Fig. S2F; Supplemental Table S2). We selected several miRNAs and measured the expression level of pri-miRNAs. We found that silencing of SYNCRIP has no significant effect on the production of pri-miRNAs (Fig. 2F), indicating SYNCRIP does not regulate miRNAs at the transcriptional level.

To validate the results from miRNA microarray, we measured the expression of corresponding mature miRNAs processed from pri-miRNAs by real-time PCR. We observed significant increase on the expression of miR-3138, miR-181a-3p, with one miRNA (miR-130-3p) showing an increase but not significant, in response to SYNCRIP knockdown. Conversely, knockdown of SYNCRIP significantly diminishes the expression of a subset of miRNAs, with miR-7-5p showing the most differentiated (Fig. 2G). This result is closely consistent with that from miRNA microarray. Among those miRNAs, we chose miR-7-5p and miR-1307 for further validation based on microRNA microarray data. The results are remarkably similar to that from let-7a-5p that: (i) Knockdown of SYNCRIP decreases the expression of mature miRNAs; (ii) overexpression of SYNCRIP increases the expression of mature miRNAs (Fig. 2H,I). Our data demonstrated that SYNCRIP is capable of regulating the expression of a subset of miRNAs, suggesting that it is a promising regulator for miRNA biogenesis.

To explore whether decreased or increased expression of miRNAs regulated by SYNCRIP are functional, we measured the expression level of let-7a miRNA as well as miR-7-5p targets which are HMGA2 and EGFR, respectively. The qPCR analysis showed that knockdown of SYNCRIP leads to increased, while overexpression of SYNCRIP leads to decreased expression of these two candidate proteins (Fig. 2J,K), suggesting that the miRNAs regulated by SYNCRIP are functional.

SYNCRIP is associated with the microprocessor and enhances microprocessor-mediated processing

To investigate the molecular mechanisms that underpin SYNCRIP-mediated regulation on miRNA biogenesis, we focused on endoribonucleases involved in two sequential processing steps subsequent to transcription, and AGO2 loading. Therefore, we studied the protein–protein interaction to explore the exact stage where SYNCRIP participates. We observed that DGCR8, Drosha specifically interact with SYNCRIP while not with eGFP (Fig. 3A); however, Dicer was not detected in FLAG-SYNCRIP immunoprecipitates (Supplemental Fig. S3A). In addition, the reciprocal Co-IP assay showed that SYNCRIP is contained in Drosha and DGCR8 immunoprecipitates, albeit its interaction with Drosha is much weaker than that with DGCR8 (Fig. 3B), suggesting that the interaction between SYNCRIP and Drosha is indirect. To gain further insights on these interactions, GST-pull down assay was used, and we found that GST-SYNCRIP is able to pull down DGCR8 not Drosha, suggesting that SYNCRIP has direct interaction with DGCR8 but not with Drosha (Fig. 3C). To further confirm whether the interaction between SYNCRIP and DGCR8 is relied on RNA, we repeated Co-IP assay with an additional step of RNase digestion. However, the interaction is still observed in the presence of RNase (Fig. 3D), confirming that RNA is not required for maintaining the interaction between SYNCRIP and DGCR8.

To elucidate the interaction in more detail and characterize the interface, Co-IP assay was performed with HEK293 cells overexpressed with myc-SYNCRIP and FLAG-tagged wild-type (1–773aa), ΔC290 (1–483aa), and ΔN483 (484–773aa) DGCR8 constructs. We found that the amino-terminal region of DGCR8 is important for the interaction with SYNCRIP (Fig. 3E), which supports the data that SYNCRIP may have indirect interaction with Drosha since Drosha interacts with the carboxyl terminus of DGCR8 (Nguyen et al. 2015). Additionally, we defined the interface of SYNCRIP with DGCR8 using GST pull-down assay. It showed that both the amino-terminal and carboxy-terminal truncated form of SYNCRIP possess the capability to interact with DGCR8 (Fig. 3F). Also, the interaction of two mutants with DGCR8 is much stronger than that of wild type, which may be due to the poor stability of the wild-type SYNCRIP. When we examined the interaction between SYNCRIP truncations and DGCR8 in living cells, we first examined the localization of SYNCRIP mutants. By immunostaining, we observed that full-length SYNCRIP mainly localizes in the nucleus as previously reported, while a portion of ΔC mutants are not able to shuttle back to the nucleus. To make SYNCRIP mutants properly localized in the nucleus as full-length SYNCRIP, we added the nuclear localization signal (NLS) from the carboxyl terminus of SYNCRIP artificially and we observed that the localization of the carboxy-terminal-truncated mutant with NLS is similar to that of the wild type (Supplemental Fig. S3C). In this scenario, we performed Co-IP to figure out the interface of SYNCRIP with DGCR8. We found that amino-terminal and carboxy-terminal truncated mutants still interact with DGCR8, indicating that the central RRMs might contribute to interacting with DGCR8 to a large extent. Additionally, artificially adding the NLS to the carboxy-terminal truncated mutant strongly enhances the interaction with DGCR8 (Supplemental Fig. S3D), implying the amino terminus still solidifies the interaction between SYNCRIP and DGCR8. Altogether, these results lead us to speculate that SYNCRIP may interact with the microprocessor and enhance microprocessor-mediated processing to augment the expression of let-7a.

To substantiate that SYNCRIP could facilitate microprocessor-mediated processing, we performed an in vitro cleavage assay using an immunoprecipitated microprocessor from HEK 293 cells overexpressed with Drosha and DGCR8 with FLAG tag, and examined the effect of SYNCRIP knockdown in microprocessor-mediated processing. Using northern blotting, we observed that the intensity of pre-let-7a-1 band slightly decreased when incubated with SYNCRIP-knockdown immunoprecipitates (Fig. 3G; Supplemental Fig. S3E). However, this defect was dramatically rescued when purified rSYNCRIP was supplemented in a dose-dependent manner (Fig. 3G). We also used pri-miR-181 as another substrate. However, no significant effect was observed on pri-miR-181 processing in the context of SYNCRIP knockdown or rescue with increasing amount of rSYNCRIP (Supplemental Fig. S3F). This suggests an alternative role of SYNCRIP in miRNA maturation, which is independent of the microprocessor, while it may participate in RISC assembly since SYNCRIP partially localizes to the cytoplasm and interacts with AGO2 (Supplemental Fig. S3B). This finding confirmed that SYNCRIP could promote microprocessor-mediated cleavage on pri-let-7a-1.

SYNCRIP binds to the terminal loop of let-7a primary transcripts

To elucidate the molecular basis underlying accelerated processing efficiency triggered by SYNCRIP, we decided to identify the binding site of SYNCRIP on let-7a precursors. A number of studies have shown that the terminal loops serve as hotspots for RBPs binding. Thus, we examined the importance of the terminal loop for interaction with SYNCRIP. To this end, we created mutants where the terminal loops were replaced with GCAA as shown in a previous study (Michlewski and Cáceres 2010), for both pri-let-7a-1 and pri-let-7a-2. Using an in vitro RNA affinity assay, we observed that the binding strikingly decreased with the RNA mutants (Fig. 4A), suggesting that the interaction can be mapped to the loop region, no matter whether it is pri-let-7a-1 or pri-let-7a-2. To further confirm

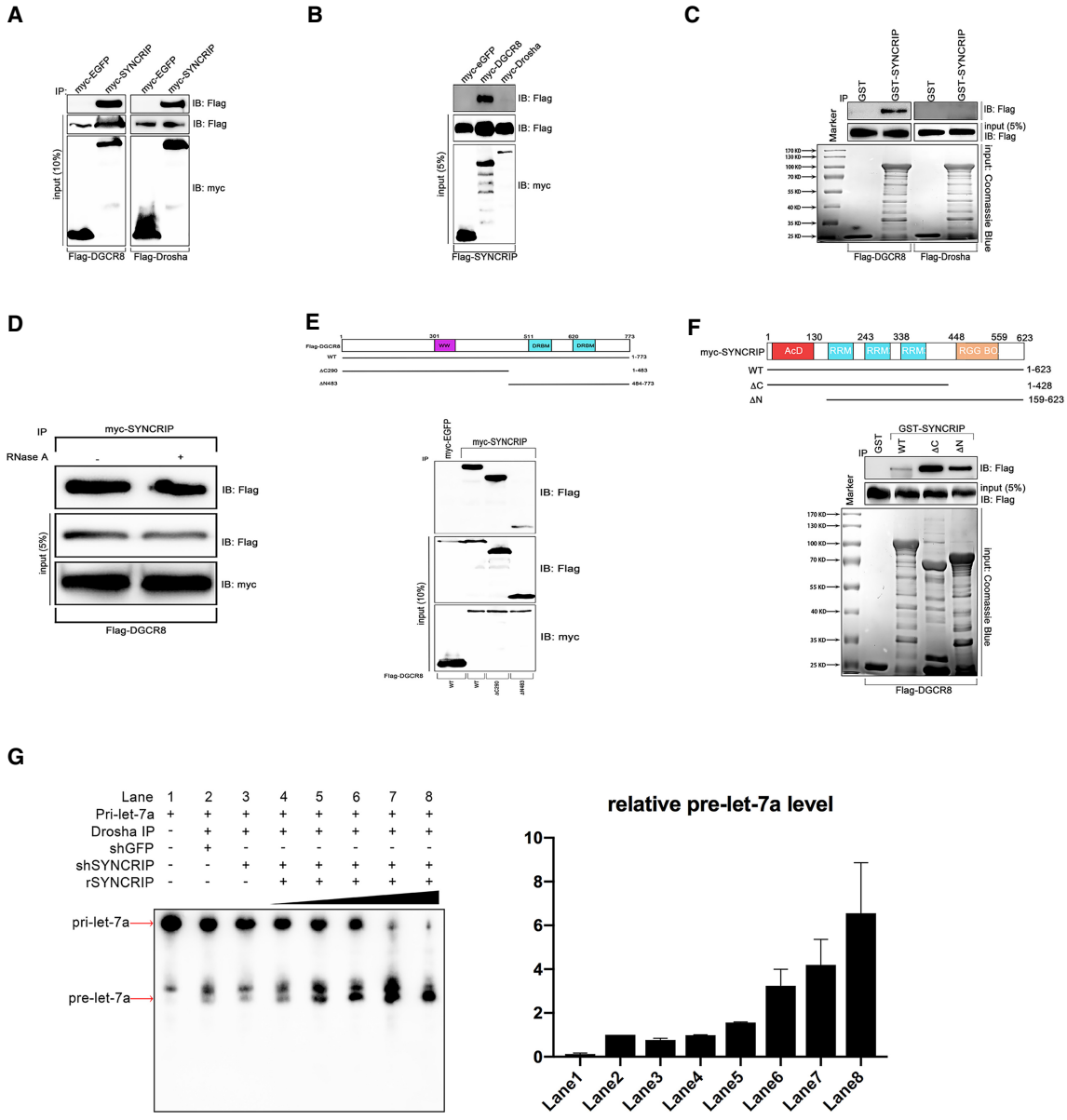

FIGURE 3. SYNCRIP associates with microprocessor complex and promotes pri-let-7a processing. (*A*) Identification of the interaction of SYNCRIP with DGCR8 and Drosha through Co-IP. Plasmid encoding FLAG-DGCR8 or FLAG-Drosha was cotransfected with plasmid expressing myc-eGFP or myc-SYNCRIP in HEK293 cells. The cell lysates were then subjected to affinity purification with anti-myc-coated beads. The immunoprecipitates were eluted and immunoblotted with indicated antibodies. (*B*) Reciprocal Co-IP in HEK293 cells cotransfected with plasmids expressing myc-eGFP, myc-DGCR8, or myc-Drosha and plasmid encoding FLAG-SYNCRIP, the cell lysates of which were incubated with anti-myc-coated beads for affinity purification, and the bound fractions were detected with indicated antibodies by immunoblot. (*C*) GST pull-down analysis using immobilized GST or GST-SYNCRIP, which was incubated with HEK293 cell lysate overexpressed with FLAG-DGCR8 or FLAG-Drosha. The bound fractions were detected by immunoblot with anti-FLAG antibodies. (*D*) Co-IP analysis of RNA dependence on the interaction between SYNCRIP and DGCR8. Immunoprecipitates containing myc-SYNCRIP were digested with RNase A (0.1 mg/mL) and subjected to immunoblot analysis against FLAG tag. (*E*) Detection of interaction between the mutants from DGCR8 and SYNCRIP in HEK293 cells. FLAG-tagged WT, carboxyl terminus truncated, or amino terminus truncated forms of DGCR8 were coexpressed with myc-tagged SYNCRIP. The cell lysates were immunoprecipitated with anti-myc-coated beads which were then immunoblotted with antibodies against FLAG. (*Top* panel) Schematic representation of domain composition of DGCR8 and its mutants. (*F*) Detection of interaction between the mutants from SYNCRIP and DGCR8. GST-tagged WT, C-terminus truncated, or amino terminus truncated forms of SYNCRIP were immobilized and incubated with cell lysates overexpressed with FLAG-DGCR8. The bound FLAG-DGCR8 was detected by western blot against FLAG. (*Upper* panel) Schematic representation of domain composition of DGCR8 and its mutants. (*G*, *left* panel) In vitro processing assay using pri-let-7a-1 as substrates. The pri-let-7a-1 substrates were incubated with FLAG-Drosha immunoprecipitates, where control shRNA (lane *2*) or SYNCRIP shRNA (lane *3*) was expressed. The reactions using immunoprecipitates where SYNCRIP was knocked down was supplemented with an increasing amount of recombinant SYNCRIP as indicated (lanes *4*–*8*). (*Right* panel) Relative processing products were quantified by Image Lab software (Bio-Rad), and error bars were presented as mean ± SEM.

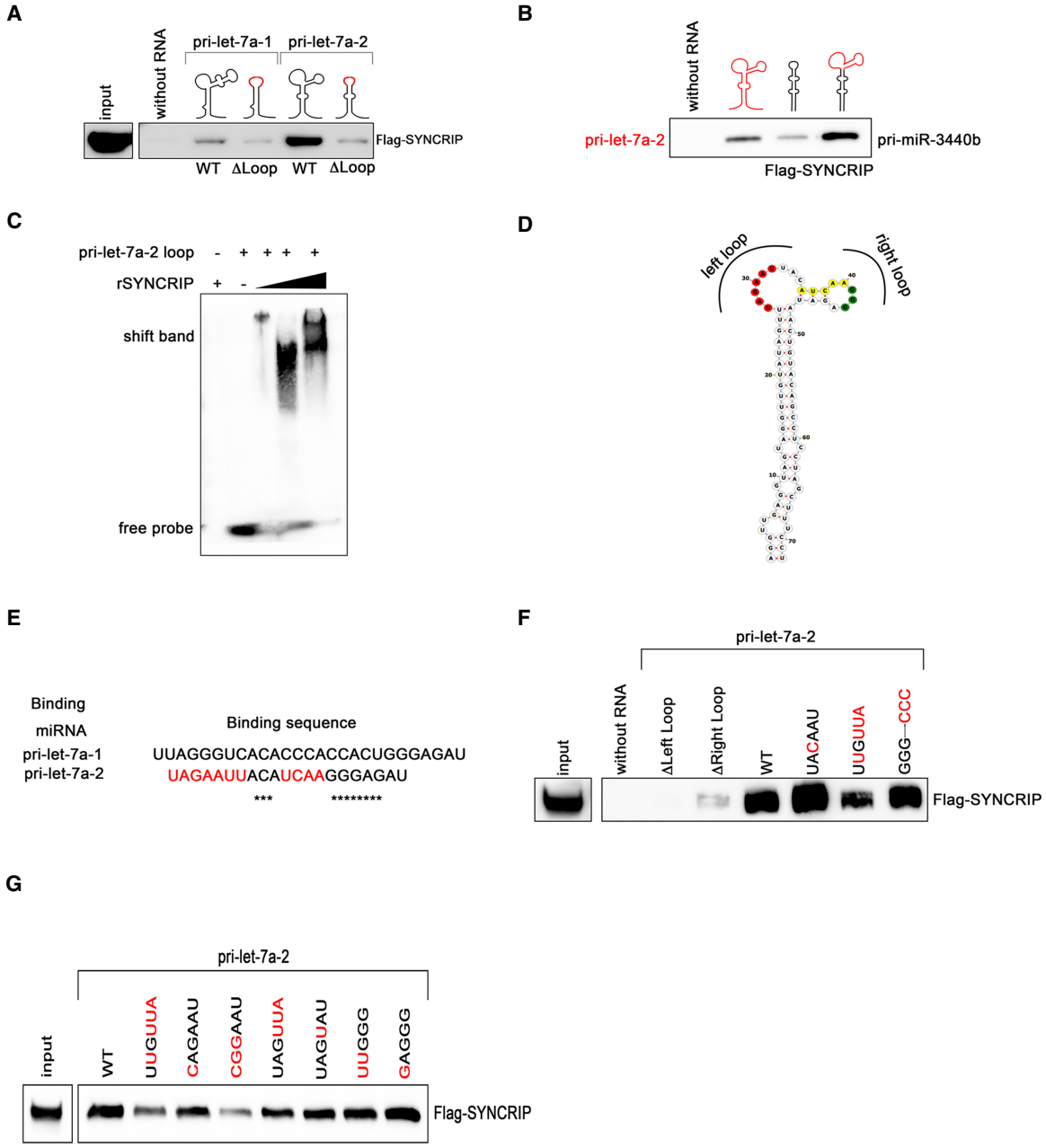

FIGURE 4. The terminal loop of pri-let-7a serves as binding site for SYNCRIP. (*A*) In vitro RNA affinity assay of overexpressed FLAG-SYNCRIP with wild-type pri-let-7a-1 or pri-let-7a-2 or their mutants where the terminal loops were replaced with GCAA. The bound fractions were immunoblotted against FLAG-tag. (*B*) In vitro RNA affinity assay of FLAG-SYNCRIP with wild-type pri-let-7a-2 or pri-miR-3440b or chimeric pri-miRNA of which the stem region is from pri-miR-3440b while the loop region is from pri-let-7a-2. The bound fractions were immunoblotted against FLAG-tag. (*C*) RNA-EMSA assay using terminal loop sequence from pri-let-7a-2. The RNA was incubated with increasing concentration of purified recombinant his-SYNCRIP. The free RNA or bound RNA was detected by northern blot using biotin-labeled probe against the terminal loop. (*D*) A schematic representation of the predicted secondary structure of pri-let-7a-2. UAGAAU: red; AUCAAG: yellow; GGG: green. (*E*) Sequence comparison of the loop region from pri-let-7a-1 and pri-let-7a-2. (*F*) In vitro RNA affinity assay of FLAG-SYNCRIP with mutants from pri-let-7a-2. The bound fractions were immunoblotted against FLAG-tag. Mutated nucleotides are labeled in red. (*G*) In vitro RNA affinity assay of FLAG-SYNCRIP with mutants from pri-let-7a-2. The bound fractions were immunoblotted against FLAG-tag. Mutated nucleotides are labeled in red.

this, we constructed a chimeric transcript based on pri-miR-3440b, an miRNA transcript from the plant, the terminal loop of which was replaced with that of pri-let-7a-2. As expected, pri-miR-3440b presented weak interaction with SYNCRIP; however, this interaction got robustly enhanced after swapping the terminal loop with pri-let-7a (Fig. 4B). To figure out whether this interaction is direct, we performed RNA-EMSA using the loop sequence from pri-

let-7a-2 and observed that the bands shifted when incubated with purified SYNCRIP (Fig. 4C). The subsequent analytical size exclusion chromatography (SEC) of SYNCRIP in complex with the terminal loop of pri-let-7a-2 presented a peak shift (Supplemental Fig. S4A). These findings confirmed the direct interaction between the terminal loop from let-7a precursors and SYNCRIP.

Since the terminal loop sequence alone may lose secondary structure, we assumed that SYNCRIP recognizes the terminal loop based on recognized sequence. SYNCRIP recognizes wide range of RNA sequences, including AUAAUC (Chen et al. 2012), GGCU/A (Santangelo et al. 2016), and G-quadruplex structure (Williams et al. 2016). The predicted secondary structure of the terminal loop from let-7a precursors contained two loops (Fig. 4D), which prompted us to explore which loop is more important for the binding. To confirm this, we created two mutants where either loop was deleted. Deletion of either loop abrogated the binding, indicating both loops are important for binding with SYNCRIP (Fig. 4F). To narrow down and to find the recognized sequence for SYNCRIP, we targeted on UAGAAU and AUCAAG which are the differences shown between the terminal of pri-let-7a-2 and that of pri-let-7a-1 (Fig. 4E), as well as GGG on let-7a-2. Accordingly, we created a series of mutants without disrupting the predicted secondary structure. We observed that SYNCRIP showed reduced binding to the RNA mutant where UAGAAU was mutated to UUGUUA or CGGAAU, while it showed identical binding ability to the rest of the mutants (Fig. 4G). Additionally, analytical SEC confirmed the direct interaction of SYNCRIP with UUUAGAAUUA (Supplemental Fig. S4A). Taken together, our data suggested that UAGAAU on the terminal loop may serve as the mooring sequence for SYNCRIP.

RRM2–3 domain of SYNCRIP has the capability to enhance the pri-let-7a processing

The gene *SYNCRIP* encodes seven isoforms of SYNCRIP proteins which are mainly varied in their amino-terminal acidic domain or carboxy-terminal tail containing RGG box as well as NLS required for nuclear-cytoplasm shuttling, while all isoforms in common have three tandem RRMs in the center of SYNCRIP. In addition to RRMs, the acidic domain and RGG box were reported to interact with RNA (Kiledjian and Dreyfuss 1992; Hobor et al. 2018). Therefore, we attempted to identify which region may serve as a minimal functional domain as SYNCRIP. To achieve this, a list of truncations of SYNCRIP protein were prepared (Fig. 5A; Supplemental Fig. S5A). To

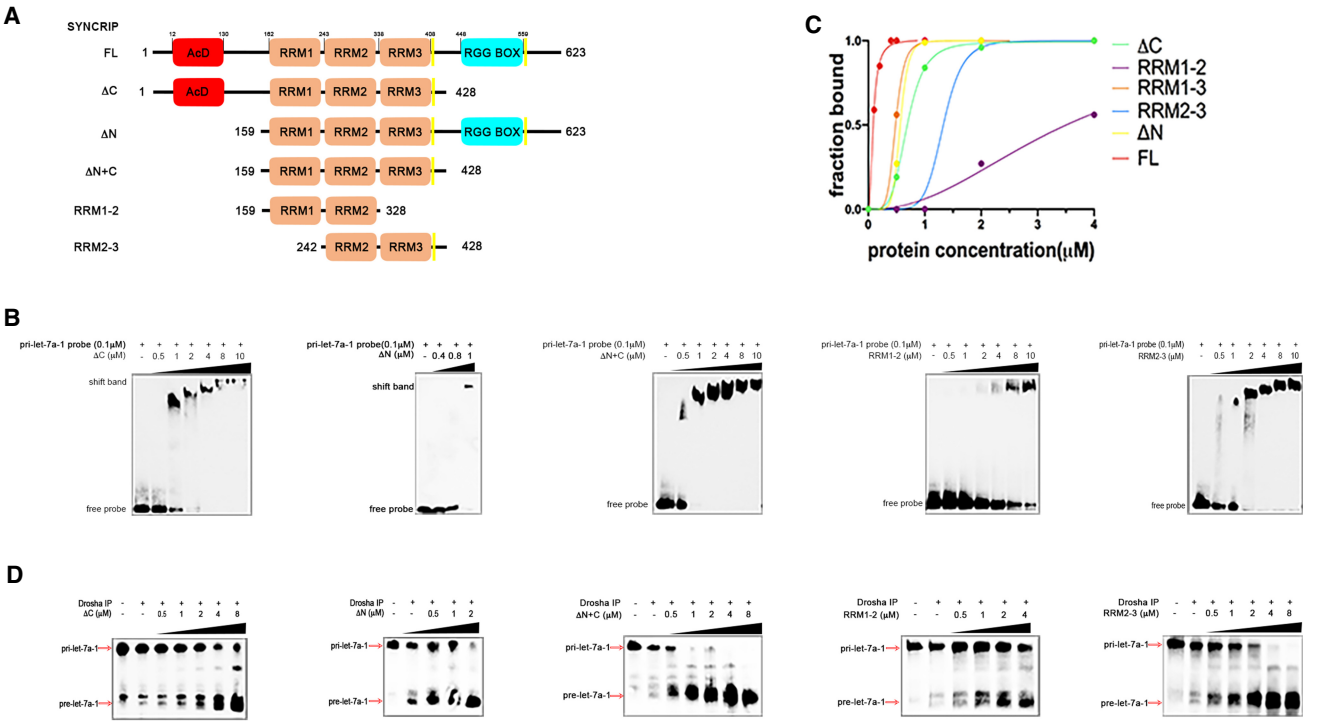

FIGURE 5. The function of SYNCRIP mutants involved in pri-let-7a interaction and processing. (*A*) A schematic representation of domain structure of SYNCRIP and the mutants. (AcD) Acidic domai, (RRM) RNA recognition motif. (*B*) RNA-EMSA assay using biotin-labeled pri-let-7a-1. Increasing concentration of purified recombinant his-ΔC, ΔN, ΔN + C, RRM1–2, RRM2–3 are indicated. (*C*) Binding affinity was analyzed by Graphpad Prism (GraphPad Software, Inc.) using a nonlinear regression model. (*D*) In vitro cleavage assay using pri-let-7a-1 as substrate. The pri-let-7a-1 was incubated with Drosha immunoprecipitates (Drosha-IP) or additionally supplemented with an increasing amount of purified recombinant SYNCRIP mutants as indicated.

roughly compare the binding affinity among the different truncations, we performed RNA-EMSA. We found that all the candidate mutants have the ability to bind RNA, whereas the affinity is varied among different mutants. Deletion of the amino terminus or carboxyl terminus or both has a similar effect of impairing the RNA binding affinity compared to the full-length protein; however, deletion of any one of the RRM domains leads to significantly lower affinity (Fig. 5B,C). We next examined whether the SYNCRIP mutants binding to the pri-let-7a has the ability to promote its processing by the microprocessor. We confirmed that the rSYNCRIP mutants themselves have no ability to process pri-let-7a into pre-let-7a, which is evident from the in vitro cleavage assay using the respective mutants (Supplemental Fig. S5B). Additionally, the in vitro processing results showed that all the mutants are capable of promoting pri-let-7a processing, suggesting that processing and the efficiency strongly correlate with the binding affinity (Fig. 5D; Supplemental Fig. S5C).

To further identify the regions required for stimulating the processing in HEK293 cells, the cells were overexpressed with truncated SYNCRIP mutants. Additionally, carboxy-terminal-truncated mutants were added with NLS artificially to compensate their impaired ability to properly localize in the nucleus. The expression of indicated proteins were detected (Supplemental Fig. S5D), and the expression level of mature let-7a was compared. We found that three tandem RRMs with NLS are capable of up-regulating let-7a miRNA, although the effect is not as strong as full-length SYNCRIP (Supplemental Fig. S5E). A previous study indicated that two tandem RRMs are sufficient for facilitating miR-18a processing in mammalian cells (Kooshapur et al. 2018), here, RRM2–3 may serve as a minimal functional domain for full-length SYNCRIP as RRM1–2 shows a lower affinity to pri-let-7a, and other domains might be required for RNA splicing or localization.

Overall structure of SYNCRIP RRM2–3 domain

As shown in Figure 5, the RRM2–3 alone is able to interact with pri-let-7a (Fig. 5B) and is capable of facilitating the processing mediated by the microprocessor in vitro (Fig. 5D). To gain insight into the molecular mechanism of both recognizing pri-let-7a and enhancing substrate processing, we determined to characterize the crystal structure of RRM2–3. RRM2–3 is composed of two tandem RRMs having a highly conserved sequence with several other RBPs among eukaryotic cells (Fig. 6A; Supplemental Fig. S6A), especially with hnRNP-R which is reported to be a nuclear counterpart of SYNCRIP and shares more than 80% of sequence similarity. The RRM2–3 structure was solved up to a resolution of 2.5 Å. After refinement, the final R_{work} and R_{free} value were improved to 18.2% and 24.9%, respectively (Supplemental Table S3). The structure (Fig. 6B; Supplemental Fig. S6B,C) shows that, each of the two RRM domains form the typical RRM structure with a β1α1β2β3α2β4 topological arrangement where four β-strands are antiparallelly arranged with two α-helices on the other side.

RRM has two highly conserved motifs, ribonucleoprotein domain 1 (RNP1) and ribonucleoprotein domain 2 (RNP2), which are important for binding to RNA. Typically, RNP2 is located along the strand β1 with a consensus sequence (Ile/Val/Leu)–(Phe/Tyr)–(Ile/Val/Leu)–X–Asn–Leu. The RNP2 sequences in RRM2 is Leu10–Phe11–Val12–Gly13–Ser14–Ile15, which differs with the consensus sequence at the last two residues. However, the RNP2 sequence in RRM3 is Leu105–Phe106–Val107–Arg108–Asn109–Leu110, which is identical to the consensus sequence. RNP1 is located near strand β3, and its consensus sequence is described as (Lys/Arg)-Gly-(Phe/Tyr)-(Gly/Ala)-(Phe/Tyr)-(Val/Ile/Leu)-X-(Phe/Tyr). The RNP1 sequence in RRM2 is Arg51–Gly52–Phe53–Cys54–Phe55–Leu56–Glu57–Tyr58 of which the fourth position is different from the consensus sequence. In RRM3, the RNP1 sequence aligns as Lys136–Asp137–Tyr138–Ala139–Phe140–Ile141–His142–Phe143. The second position is an Asp residue instead of Gly in the consensus sequence. Therefore, only RNP2 in the RRM3 domain is a canonical motif.

The structure of RRM2–3 is highly conserved as each RRM domain can be superimposed into other RRMs with low root-mean-square deviation (RMSD). Structure comparison of the RRM2 domain with mouse TDP-43 in complex with DNA (PDB entry 3D2W) showed that the alignment of 43 Cα atoms has an RMSD of 1.35 Å and the residues that are responsible for interaction with the nucleic acid are Phe194 and Phe231 via aromatic stacking. The corresponding residues in RRM2 are Phe11 and Phe55 (Fig. 6C). For RRM3, when superimposed into hnRNP A1 in complex with RNA (PDB entry 6DCL), the RMSD was calculated as 0.677 Å of total 48 Cα atoms. Similar to TDP43, the residues required for interaction with RNA in hnRNP A1 were reported to be Phenylalanine residues in RNP sequences, which are also observed in the RRM3 domain as Phe106 and Phe140 (Fig. 6D). These results suggest that the Phenylalanine residues in RNP sequences may serve as key residues for their interaction with RNA.

DISCUSSION

SYNCRIP is an evolutionarily conserved protein among eukaryotes and participates in the regulation of neuronal development, viral replication, circadian oscillation (Choi et al. 2004; Kim et al. 2007, 2010; McDermott et al. 2012). In addition, SYNCRIP has been implicated in the regulation of RNA metabolism (Kabat et al. 2009; Kim et al. 2011, 2013). However, whether SYNCRIP could regulate miRNA biogenesis remains unknown. Establishing SYNCRIP/miRNA pathway will provide new insights to explain the biological function of SYNCRIP in developmental defects or disease.

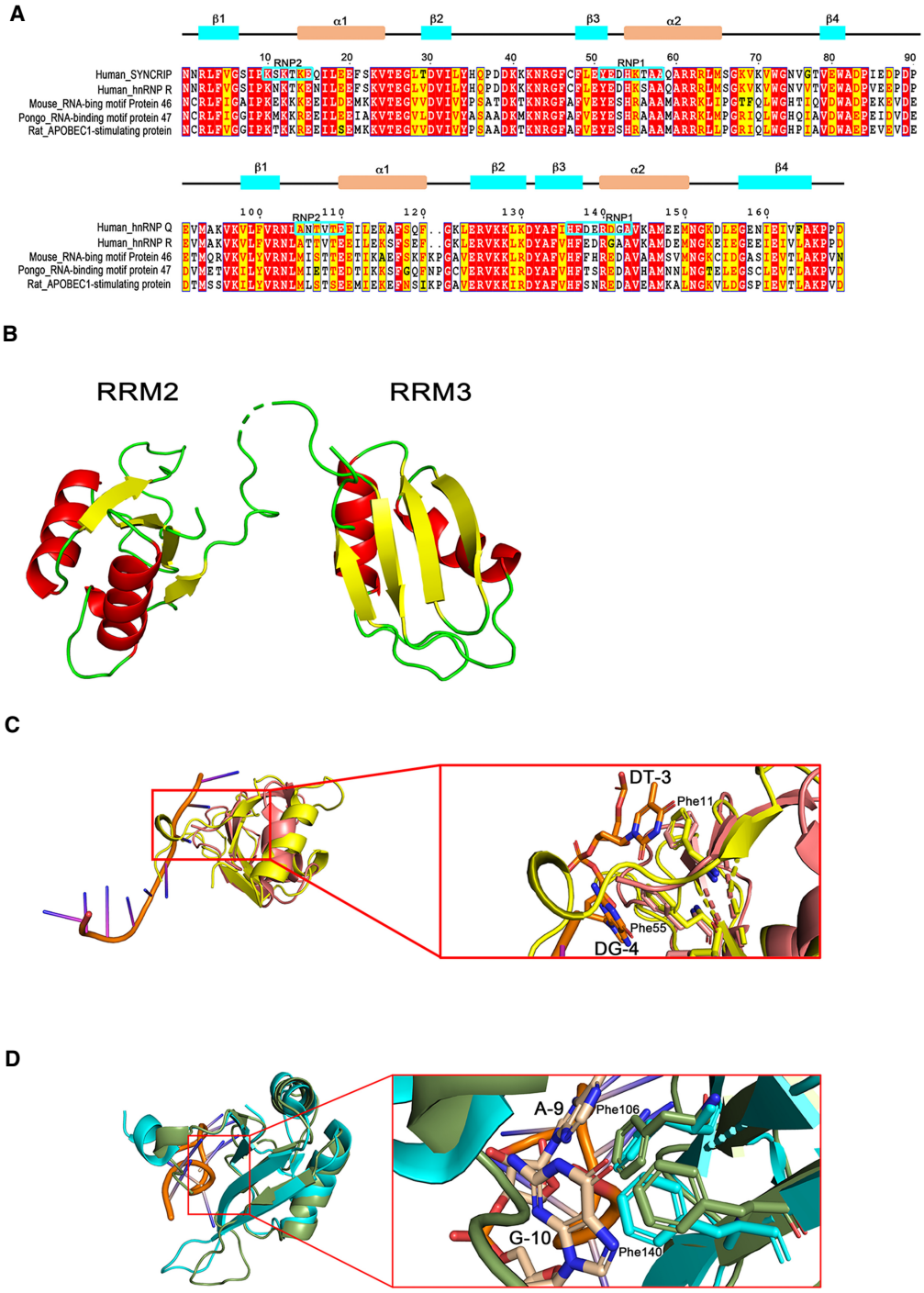

FIGURE 6. The structure of RRM2–3 from SYNCRIP. (*A*) Sequence alignment of RRM2–3 domain with various RNA binding domains from RBPs. The *upper* panel shows the secondary structure of RRM2–3. (*B*) Crystal structure of RRM2–3 at 2.5 Å resolution, showing characteristic RRM folding as β1α1β2β3α2β4 topology. (*C*) Structure alignment of SYNCRIP RRM2 domain (yellow) with mouse TDP-43 RRM2 domain (salmon; PDB entry 3D2W). (*D*) Structure alignment of SYNCRIP RRM3 (green) with human hnRNP A1 RRM 2 (cyan; PDB entry 6DCL).

In this study, we demonstrated that SYNCRIP is required to maintain the expression of let-7a, and overexpression of SYNCRIP could promote the expression of functional let-7a. This was achieved by both direct interaction with pri-mary miRNAs and protein–protein interaction with DGCR8. The interactions enhance the post-transcriptional processing of pri-let-7a (Fig. 7). Moreover, SYNCRIP is broadly involved in the regulation of a subset of miRNAs,

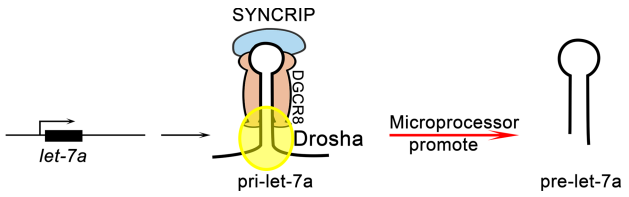

FIGURE 7. A schematic representation of the regulated processing pathway of pri-let-7a by SYNCRIP. SYNCRIP promotes pri-let-7a processing by interaction with DGCR8 and the terminal loop of pri-let-7a.

not limited to let-7a, suggesting that SYNCRIP is a new miRNA regulator.

SYNCRIP was previously identified to interact with pri-let-7a in an tRSA-RNA affinity assay. Here, we confirmed this interaction on the basis of combinatorial in vivo and in vitro studies. The results showed that SYNCRIP has direct interaction with pri-let-7a-1 as well as pri-let-7a-2. Consistently, a recent paper showed that SYNCRIP has specific interaction with pre-let-7a-2, which provides supportive evidence that SYNCRIP interacts with let-7a progenitors (Treiber et al. 2017). Of particular interest, our mutation studies revealed that SYNCRIP directly binds to the terminal loop of let-7a precursors, the recognized sequence of which includes UAGAAU that is similar to AUAAUC. The AUAAUC sequence is reported to be recognized by SYNCRIP, and this recognition regulates the localization of mRNA containing AUAAUC sequence (Chen et al. 2012). In addition to AUAAUC, SYNCRIP recognizes diverse RNA motifs, such as poly(A) (Svitkin et al. 2013), G-stretch (Williams et al. 2016), to affect RNA dynamics. However, when the G-stretch sequence embedded in the terminal loop of pri-let-7a was mutated to CCC, the affinity to SYNCRIP was not affected, confirming that GGG is not a determinant for SYNCRIP binding with pri-let-7a. Another hEXO sequence (GGCU/A) was identified as a determinant for miRNA partition to exosome mediated by SYNCRIP (Santangelo et al. 2016); however, this sequence was not observed in the terminal loop of let-7a precursors.

Although SYNCRIP is characterized to be a positive post-transcriptional regulator for pri-let-7a by facilitating the Drosha-dominant cleavage, the detailed molecular mechanism underlying enhanced processing needs to be further investigated. The structure of the RRM2–3 domain showed it to be a conserved RNA binding domain with typical β1α1β2β3α2β4 topological conformation. Structure alignment of each RRM with other RRMs from TDP43 and hnRNP A1 showed high structure similarity, suggesting the key residues including phenylalanine residues in RNP1 and RNP2 sequence and binding mode for the RRM2–3 domain with the terminal loop from pri-let-7a. hnRNP A1 was reported to be a positive regulator for mir-18a (Guil and Cáceres 2007), while a negative regulator for let-7a (Michlewski and Cáceres 2010), both by docking at the terminal loop of these miRNAs. The molecular basis of terminal-mediated regulation on miRNA is varied. The most recent study uncovered the mechanistic basis by crystal structure that each RRM domain recognizes the UAG motif embedded in the terminal loop, which induces unwinding of the stem region and further facilitates Drosha accessing to the cleavage sites (Kooshapur et al. 2018). Another mechanism would be the recruitment of DGCR8 since the UGU motif located at the terminal loop is reported to be a *cis*-element recognized by DGCR8 (Auyeung et al. 2013). Therefore, SYNCRIP may adopt one or more of these mechanisms to enhance pri-let-7a processing. However, to clearly elucidate the mechanism, structural characterization of the protein–RNA complex could be of great value.

miRNAs have been revealed to have essential biological functions since the last century, and they are intimately orchestrated by a series of RBPs according to different development stages or tissue types. Here, we have demonstrated that the knockdown or overexpression of SYNCRIP has significant effects on miRNA biogenesis as in the case of let-7 miRNA. Syp, an ortholog protein of SYNCRIP in *Drosophila*, and let-7 miRNA are required for the maturation of NMJ in *Drosophila* (Caygill and Johnston 2008; Halstead et al. 2014), thus, it is plausible that SYNCRIP may regulate NMJ development through regulating let-7 maturation. In mammalian cells, knockdown of SYNCRIP leads to 50% decrease, and overexpression of SYNCRIP leads to 50% increase in the expression of let-7 miRNA, which further regulates the expression of the target mRNA, HMGA2. In addition, 50% decrease of let-7 was shown to promote proliferation by 16% (Liu et al. 2012), indicating that the regulation of SYNCRIP on miRNA is functional. We also observed that SYNCRIP is indispensable for the expression of miR-15b-5p and miR-16-5p, and it was reported that SYNCRIP has specific interactions with pre-miR-15b and pre-miR-16-1 (Treiber et al. 2017), which further supports our results that miR-15b and miR-16-1 could be regulated by SYNCRIP. These two miRNAs were shown to be down-regulated in chronic lymphocytic leukemia (CLL) (Pekarsky and Croce 2015). Collectively, SYNCRIP could regulate the expression of these miRNAs and maintain the growth of leukemic cancer cells. In addition to let-7a, SYNCRIP positively regulates miR-7 biogenesis. miR-7 is a tissue-specific miRNA enriched in brain and pancreatic tissues (Farh et al. 2005). In other types of tissues, pri-miR-7 processing is inhibited by HuR/MSI2 (Choudhury et al. 2013). HuR recognizes the terminal loop of pri-miR-7 and mediates the recruitment of MSI2, which blocks pri-miR-7 processing in non-neuron cells. Since SYNCRIP can regulate maturation of NMJ formation in *Drosophila* and the length of axons or numbers of dendrites as well as neuron morphogenesis in mammalian cells (McDermott et al. 2014), it is plausible

that SYNCRIP could exert its function by regulating the production of let-7 miRNA or miR-7-5p in neuron development. In conclusion, our studies identified SYNCRIP as a new miRNA regulator that promotes biogenesis of several miRNAs. This opens up a new layer of regulation on miRNA and gives new insights into miRNA-related diseases.

MATERIALS AND METHODS

Cell culture

Human HEK293 cells were cultured in Dulbecco's modified Eagle medium (DMEM, Gibco) supplemented with 10% fetal bovine serum (FBS, Hyclone), 100 unit/mL penicillin, 100 µg/mL streptomycin (Gibco). Cells were maintained at 37°C in the presence of 5% CO_2.

Transfection

Human HEK293 cells were transfected with plasmids using polyethylenimine (PEI, Polysciences) as a transfection reagent. Once the cells grew to 80%–90% confluency, transfection was performed with the ratio of plasmid to PEI as 1:2. After 48 h post-transfection, the cells were washed with phosphate buffered saline (PBS) before proceeding to the downstream experiments.

Construction of vectors used in this study

To achieve efficient knockdown of SYNCRIP, we used pSuper vector to express shRNA. To overexpress SYNCRIP in HEK293 cells, we used pXJ40-myc or pXJ40-FLAG vector, which expresses fusion protein with myc or FLAG tag at the amino terminus. To overexpress pri-miRNA in living cells, we used modified pcDNA5/tRSA. pET28b or pGEX-6P-1 were used to express SYNCRIP in *Escherichia coli* with His or GST tag, respectively. All the primers used for construct preparation have been listed in the Supplemental Material.

Expression and purification of recombinant proteins

All proteins used for biochemical assays or crystallography were expressed in *E. coli* strain BL21 (DE3) by induction with 0.4 mM IPTG when the value of OD_{600} reached ~0.6, followed by incubation for 16 h at 20°C. The bacteria cultures were harvested and resuspended in lysis buffer (25 mM Tris-HCl [pH 7.4], 25 mM KH_2PO_4 [pH 6.8], 10% Glycerol, 500 mM NaCl and 1 mM DTT) supplemented with 1 mM phenyl-methyl-sulfonyl fluoride (PMSF). The suspension was lysed using high-pressure homogenizer and the cell debris was removed by ultracentrifugation (Beckman Coulter). For His-tagged proteins used in the biochemical assays, the supernatant was loaded to Nickel-charged immobilized metal affinity chromatography (IMAC) columns (HisTrap HP, GE Healthcare) preequilibrated with EQ buffer (10 mM Tris-HCl [pH 7.4], 10% glycerol, and 250 mM NaCl). The proteins in this study were all eluted at the 250–500 mM imidazole concentrations. The protein-containing fractions were pooled and applied on a HiLoad 26/60 Superdex 75 gel filtration column (GE Healthcare) equilibrated with GF buffer (25 mM Tris-HCl [pH 7.4], 500 mM NaCl, 4 mM DTT, and 0.5 mM EDTA). Peak fractions containing target proteins were pooled and dialyzed into a buffer containing 25 mM Tris-HCl (pH 7.4), and 100 mM NaCl for full-length, ΔC, ΔN + C, RRM1–2, RRM2–3 of SYNCRIP, or buffer containing 25 mM Tris-HCl (pH 7.4), and 500 mM NaCl for ΔN of SYNCRIP overnight. Aliquots were stored at −80°C. For GST-tagged proteins used in GST pull-down assay, the supernatant was loaded to GSTrap HP Columns (GE Healthcare) preequilibrated with EQ buffer. The proteins bound to the GST column were eluted with GST Elute Buffer (50 mM Tris-HCl [pH 8.0], 20 mM reduced Glutathione). The protein-containing fractions were pooled and dialyzed to buffer (25 mM Tris-HCl [pH 7.4], 500 mM NaCl) overnight. Aliquots were stored at −80°C. To purify the RRM2–3 domain for crystallography, after eluting from HisTrap HP columns, fractions containing proteins were pooled, added with thrombin protease to remove His tag, and then dialyzed to a buffer containing 25 mM Tris-HCl (pH 7.4) and 100 mM NaCl for 2 d. After that, the samples were loaded onto the HisTrap HP columns a second time to remove the His-tag. The samples were subsequently applied on a HiLoad 26/60 Superdex 75 gel filtration column, and peak fractions containing proteins were pooled and dialyzed into a buffer containing 25 mM Tris-HCl (pH 7.4) and 100 mM NaCl overnight. On the next day, protein samples were concentrated to 10 mg/mL and used for crystallization screening.

Protein crystallization and structural determination

The RRM2–3 domain was successfully crystallized in a buffer consisting of 0.1 M HEPES/sodium hydroxide (pH 7.5) and 20% PEG 10,000. The crystals were flash frozen in liquid nitrogen. The data were collected with the Rigaku X-Ray system in the X-Ray Crystallography Facility in the Department of Biological Sciences, National University of Singapore. A total of 180 frames were collected at a 1° oscillation for the crystal. The data sets were processed and scaled with the HKL2000 program (Otwinowski and Minor 1997). The structure was determined by molecular replacement using the Molrep program (Navaza and Saludjian 1997). The structure of the RBP domain in SYNCRIP (PDBID: 2DGU) was used as the model. Final model building was carried out using the *Coot* program (Emsley and Cowtan 2004) and refined using Phenix-refine (Adams et al. 2010).

Analytical size-exclusion chromatography

One of the SYNCRIP mutants, RRM2–3, was used to analyze the binding capability to sequence on a let-7a precursor; therefore, three samples were prepared accordingly: native protein, protein incubated with 21 nt RNA (5′-UAGAAUUACAUCAAGGGAGAU-3′), and protein incubated with 10 nt RNA (5′-UUUAGAAUUA-3′). After incubation in RNA-EMSA buffer for 1 h, these samples were applied on Column Superdex 200 Increase 10/300 GL (GE Healthcare) for size exclusion with 0.2 mL/min. Before each round of sample injection, the column was washed with 0.2 M NaOH to clear out remaining proteins followed by equilibration with RNA-EMSA buffer (20 mM HEPES-KOH [pH 8.0], 150 mM KCl, 1.5 mM $MgCl_2$, 0.2 mM EDTA, 0.1% [w/v] Triton X-100). All operations were run at 4°C.

In vitro transcription

To generate RNA for in vitro RNA affinity assay, in vitro cleavage assay, the corresponding DNA sequences were constructed into pcDNA5 vectors and sequenced. Subsequently, the vectors were used as templates in PCR reactions to amplify the templates for in vitro transcription. In vitro transcriptions were performed using the Large Scale RNA Production System-T7 (Promega) according to the manufacturer's instructions. To further generate an RNA probe for RNA-EMSA assay, the in vitro transcribed RNAs were labeled with biotin according to the manufacturer's instructions.

tRSA-RNA affinity assay

The tRSA-RNA affinity assay was carried out based on previous studies (Iioka et al. 2011). HEK293 cells were cotransfected with plasmids encoding FLAG-SYNCRIP and plasmids expressing pcDNA5/tRSA-pri-let-7a or pcDNA5/tRSA (negative control). After 72 h post-transfection, cells were harvested and incubated in lysis buffer containing 50 mM Tris-HCl (pH 8.0), 150 mM KCl, 0.5% Triton-X 100, and 10% glycerol, supplemented with 2 mM β-Mercaptoethanol, Protease Inhibitor Cocktail (Roche), RiboLock RNase Inhibitor (40 U/μL; Thermo Fisher Scientific) on ice for 20 min followed by sonication and centrifugation twice for 10 min at 4°C. The supernatant was then incubated with 50 μL streptavidin-coated Sepharose beads (GE Healthcare) with constant rotation for 6 h at 4°C. The beads were washed four times with lysis buffer followed by five times with wash buffer containing 20 mM Tris-HCl (pH 8.0), 300 mM KCl, and 0.2 mM EDTA. After washing, the bound proteins were eluted with 2× SDS loading buffer and immunoblotted with the respective antibodies.

In vitro RNA affinity assay

pri-let-7a-1 and pri-let-7a-2 with 5′ short extension were generated by in vitro transcription. A 3′-biotinylated adaptor DNA, the sequence of which is reverse-complementary to the 5′ extension, was incubated with Streptavidin-coated Sepharose beads in binding buffer containing 20 mM Tris-HCl (pH 7.5), 100 mM KCl, and 2 mM EDTA at 4°C with constant rotation for 1 h. The beads were washed twice with wash buffer (20 mM Tris-HCl [pH 8.0], 300 mM KCl, 0.2 mM EDTA) and incubated with in vitro transcribed pri-miRNAs in the wash buffer supplemented with Ribolock RNase Inhibitor for 3 h at 4°C with constant rotation. The beads were washed twice with wash buffer followed by once with lysis buffer and incubated with cell lysates. The cell lysates were prepared using the same methods as tRSA-RNA affinity assay. The sequences for RNA bait are listed in Supplemental Table S4.

RNA-EMSA

Biotin-labeled pri-let-7a-1 probe was generated by in vitro transcription followed by biotin-labeling with EZ-Link NHS-Biotin (ThermoFisher). A total of 1 pmol of biotin-labeled RNA probes was incubated with increasing concentrations of purified recombinant protein expressed in *E. coli* in reaction buffer (20 mM HEPES-KOH [pH 8.0], 150 mM KCl, 1.5 mM $MgCl_2$, 0.2 mM EDTA, 0.1% [w/v] Triton X-100) at 4°C for 1 h. After the reaction, the samples mixed with loading buffer (10 mM Tris-HCl, 3% [w/v] sucrose and dyes) were loaded on 8% (w/v) native gel and run at a constant voltage of 100 V. After electrophoresis, the probe was transferred onto hybond-N+ membrane and detected using Chemiluminescent Nucleic Acid Detection Module Kit (ThermoFisher).

RNA-immunoprecipitation assay (RIP)

HEK293 cells were transfected with plasmids expressing FLAG-SYNCRIP or FLAG-eGFP (negative control). After 72 h after transfection, cells were harvested and resuspended in lysis buffer (10 mM HEPES-KOH [pH 7.4], 100 mM KCl, 5 mM $MgCl_2$, 0.5% NP-40) supplemented with 2 mM β-Mercaptoethanol, Protease Inhibitor Cocktail (Roche), Ribolock RNase Inhibitor (40 U/μL; Thermo Fisher Scientific) on ice for 20 min followed by sonication and centrifugation twice for 10 min at 4°C. After centrifugation, 10% of the supernatant was used as the input for RT-PCR or RT-qPCR analysis. The rest of the supernatants were incubated with anti-FLAG antibody-conjugated agarose beads (anti-FLAG M2 affinity gel, Sigma) with constant rotation for 4 h at 4°C. The beads were washed four times with lysis buffer and then five times with wash buffer (50 mM Tris-HCl [pH 7.4], 150 mM NaCl, 1 mM $MgCl_2$, 0.05% NP-40). After washing, the beads were incubated with the lysis buffer containing proteinase K for 30 min at 55°C. After centrifugation, RNA was recovered from samples, including input and immunoprecipitates (IP), using the TRIzol method. Prior to reverse transcription, the extracted RNA was treated with DNase I (Sigma). Reverse transcription was performed using Random Hexamer Primer (ThermoFisher). RIP–PCR was performed using the primers listed in Supplemental Table S1. RIP–qPCR was performed using the qPCR primer for pri-let-7a-1.

RNA isolation and miRNA microarray

miRNA microarray was performed using a SYNCRIP shRNA-treated RNA sample compared to the control shRNA-treated RNA sample. The total RNA was extracted from HEK293 cells using miRNeasy Mini Kit (Qiagen) according to the manufacturer's instructions. Total RNA samples were sent to Axil Scientific for miRNA microarray analysis. One microgram of total RNA was labeled with FlashTag Biotin HSR Labeling Kit before being hybridized to GeneChip miRNA 4.0 Array (Affymetrix, Inc.), which consists of 30,434 mature miRNA probe sets. The array was scanned using the GeneChip Scanner and the data exported and processed using the Affymetrix Expression Console Software.

Quantitative real-time PCR

cDNA was synthesized by revertaid Reverse Transcriptase (RT, ThermoFisher) according to the provided protocol. Oligo(dt)15 primers were used as the RT primers for reverse transcription of mRNAs and pri-miRNAs. miRNA-specific stem–loop primers were used as RT primer for reverse transcription of mature miRNAs. qPCR was carried out in the CFX96 Touch Real-Time PCR Detection System (BioRad). Quantification of mRNAs and pri-miRNAs was performed using Luminaris HiGreen qPCR Master Mix (ThermoFisher). Quantification of mature miRNA was performed using Luminaris Probe qPCR Master Mix (ThermoFisher),

as well as Universal Probe Library probe 21 (Roche). All measurements were done in triplicates. All the primers are listed in Supplemental Table S1.

Northern blot analysis

Thirty micrograms of total RNA was separated in 20% denaturing PAGE gels. The resolved RNA was transferred onto Hybond-N+ membranes at 100 V at 4°C for 30 min. After UV cross-linking, blocking was carried out using ULTRAhyb Ultrasensitive Hybridization Buffer (Invitrogen) for 2 h followed by addition of 5′ biotin-labeled DNA probe and incubation for 20 h, as indicated by the manufacturer's instructions. The blots were further proceeded to Chemiluminescent Nucleic Acid Detection Module Kit, and the signal was detected by ChemiDoc Imaging System (Bio-Rad).

Coimmunoprecipitation assay

Forty-eight hours after transfection with the indicated plasmids, HEK293 cells were harvested and lysed with Co-IP lysis buffer (20 mM Tris [pH 8.0], 137 mM NaCl, 1 mM EDTA, 1.5 mM $MgCl_2$, 10% glycerol, 1% Triton X-100) supplemented with 2 mM β-Mercaptoethanol, Protease Inhibitor Cocktail (Roche). After incubation on ice for 20 min, the cells were further sonicated followed by centrifugation twice for 10 min. Ten percent of the supernatant was taken as input and the rest of the supernatants were incubated with 20 µM of anti-c-myc affinity gel (Sigma) with constant rotation at 4°C for 4 h. After incubation, the beads were washed three times with Co-IP lysis buffer and another five times with Co-IP wash buffer (20 mM Tris [pH 7.5], 300 mM NaCl, 2.5 mM $MgCl_2$, 0.5% NP-40). The bound proteins on myc beads were eluted with 2× SDS loading buffer by boiling for 10 min and analyzed by western blot.

Western blot analysis

Protein samples were separated by SDS-PAGE and transferred to polyvinylidene difluoride (PVDF) membrane (Bio-Rad). Membranes were immunoblotted with primary anti-c-myc antibodies (Sigma) or anti-FLAG antibodies (Sigma) followed by secondary horseradish peroxidase-conjugated (HRP) anti-mouse IgG (GE Healthcare). Immobilon Western Chemiluminescent HRP Substrate (Merck Millipore) was used for signal detection by ChemiDoc Touch Gel Imaging System (Bio-Rad).

GST pull down

Approximately five micrograms of purified GST or GST fusion proteins were incubated with glutathione-Sepharose beads (GE healthcare) at 4°C for 1 h. After washing out the extra proteins using binding buffer (25 mM Tris [pH 7.4], 500 mM NaCl, 4 mM DTT) three times, the beads were incubated with cell lysate overexpressed with FLAG-DGCR8 or FLAG-Drosha for 4 h at 4°C with rotation. The cell lysates were prepared with the same method as Co-IP assay. After incubation, the beads were washed three times with Co-IP lysis buffer followed by four times with Co-IP wash buffer and resuspended in 30 µL of 2× SDS loading buffer. The protein sample was then analyzed with western blot.

In vitro processing assay

In vitro processing assays were carried out according to previous studies (Lee et al. 2003). Briefly, HEK293 cells were cotransfected with plasmids encoding FLAG-Drosha and FLAG-DGCR8 and plasmids expressing SYNCRIP shRNA or control shRNA. Forty-eight hours after transfection, the cells were harvested and lysed on ice for 20 min in lysis buffer (20 mM HEPES-KOH [pH 7.5], 150 mM NaCl, 0.2 mM EDTA, 5% glycerol). After on ice lysis, the cells were further sonicated briefly and centrifuged for 10 min twice. The supernatant was incubated with anti-FLAG antibody-conjugated agarose beads (anti-FLAG M2 affinity gel, Sigma) with constant rotation for 4 h at 4°C. After incubation, the beads were washed five times with lysis buffer and the bound fractions were eluted with 3×FLAG peptide (Genscript) in lysis buffer. Processing reactions were carried out in reaction buffer (20 mM Tris-HCl [pH 8.0], 6.4 mM MgCl2, 1 mM ATP, 10% glycerol, 0.2 mg/mL BSA) supplemented with 1 unit/µL of Ribolock RNase Inhibitor (ThermoFisher). In each reaction, 1 µM of in vitro transcribed pri-let-7a-1 was incubated with 2.5 µL of Drosha immunoprecipitates (Drosha-IP), different concentrations of purified recombinant His-SYNCRIP or its mutants and NaCl were supplemented to the final concentration of 100 mM. The reaction was incubated at 37°C for 90 min. RNA was recovered from the reaction using phenol:chloroform:isoamyl alcohol followed by ethanol precipitation and separated by 12.5% denaturing UREA-PAGE gel. After electrophoresis, the resolved RNA was transferred to Hybond-N+ membranes and detected by northern blot as described above.

Biolayer interferometry (BLI)

The Octet RED96 (ForteBio, Pall) was used to measure the binding affinity of SYNCRIP and Biotin-labeled pri-let-7a. Two hundred microliters of reaction experiments were set up in black 96-half well plates and performed at 37°C. Streptavidin biosensor tips (Pall) were hydrated in 200 µL of reaction buffer (50mM Tris pH 6100 mM NaCl, 0.1% Tween-20,1 mg/mL BSA) for 15 min. After a baseline step of 120 sec, RNA was immobilized on the streptavidin biosensors at a concentration of 80 nM for 10 min. A second baseline step of 120 sec was followed, to wash unbound RNA and allow signal stabilization. Association was monitored by transferring the ligand biosensors to wells containing the recombinant proteins in a concentration of 80, 100, and 120 nM. The association and dissociation was 5 min, respectively. A final regeneration cycle was performed to strip the biotin-labeled RNA and allow for one subsequent rebinding. The sensor was dipped in regeneration buffer (1 M glycine pH 1.7) for 120 sec, followed by 240 sec in reaction buffer. Binding interactions in solution caused the optical density of the biosensor to change, resulting in a wavelength shift proportional to binding. Data were taken for each protein and were analyzed using the ForteBio Data Analysis 9.0 software. The reference sensors were used for each concentration of protein to subtract the nonspecific binding. The *y*-axes of all steps were aligned to each step's baseline, and curve fitting was performed to analyze the data. Curve

fitting and KD value determination were calculated using both the association and dissociation steps and a 1:1 global fitting model. The K_D values represent the affinity constant and thus represent an equilibrium state. The k_{on} and k_{off} rates are used to predict the equilibrium state of the interaction, and how quickly the system responds to changes in concentration of the protein. The k_{on} values represent the rate of association, or the rate at which the complex forms. The k_{off} values represent the rate of dissociation, or the rate at which the complex disassembles during equilibrium. Only fitted curves with an R^2 value of 0.98 or greater were used in the analysis.

DATA DEPOSITION

Atomic coordinates and structure factors for the reported crystal structures have been deposited with the Protein Data bank under accession number 6KOR.

SUPPLEMENTAL MATERIAL

Supplemental material is available for this article.

ACKNOWLEDGMENTS

We are grateful for invaluable comments from Dr. Satoru Machida on this study. We acknowledge support from Professor J. Sivaraman for sharing his laboratory facilities for this study. This work was supported by a grant from the Ministry of Education Singapore (R154-000-A39-112).

Author contributions: Y.C., W.C., and Y.A.Y. participated in experimental design and data analysis. Y.C. and M.S. carried out the experiments. J.C., J.L., and C.J. participated in structure determination and data analysis. G.S.K. and Y.-K.M. performed the BLI experiments and analysis, respectively. Y.C. and C.J. wrote the manuscript.

Received August 17, 2019; accepted December 22, 2019.

REFERENCES

Adams PD, Afonine PV, Bunkóczi G, Chen VB, Davis IW, Echols N, Headd JJ, Hung LW, Kapral GJ, Grosse-Kunstleve RW, et al. 2010. PHENIX: a comprehensive Python-based system for macromolecular structure solution. *Acta Crystallogr D Biol Crystallogr* **66:** 213–221. doi:10.1107/S0907444909052925

Auyeung VC, Ulitsky I, McGeary SE, Bartel DP. 2013. Beyond secondary structure: primary-sequence determinants license pri-miRNA hairpins for processing. *Cell* **152:** 844–858. doi:10.1016/j.cell.2013.01.031

Bartel DP. 2009. MicroRNAs: target recognition and regulatory functions. *Cell* **136:** 215–233. doi:10.1016/j.cell.2009.01.002

Bashirullah A, Pasquinelli AE, Kiger AA, Perrimon N, Ruvkun G, Thummel CS. 2003. Coordinate regulation of small temporal RNAs at the onset of *Drosophila* metamorphosis. *Dev Biol* **259:** 1–8. doi:10.1016/S0012-1606(03)00063-0

Bohnsack MT. 2004. Exportin 5 is a RanGTP-dependent dsRNA-binding protein that mediates nuclear export of pre-miRNAs. *RNA* **10:** 185–191. doi:10.1261/rna.5167604

Caygill EE, Johnston LA. 2008. Temporal regulation of metamorphic processes in *Drosophila* by the let-7 and miR-125 heterochronic microRNAs. *Curr Biol* **18:** 943–950. doi:10.1016/j.cub.2008.06.020

Chen HH, Chang JG, Lu RM, Peng TY, Tarn WY. 2008. The RNA binding protein hnRNP Q modulates the utilization of exon 7 in the survival motor neuron 2 (*SMN2*) gene. *Mol Cell Biol* **28:** 6929–6938. doi:10.1128/MCB.01332-08

Chen HH, Yu HI, Chiang WC, Lin YD, Shia BC, Tarn WY. 2012. hnRNP Q regulates Cdc42-mediated neuronal morphogenesis. *Mol Cell Biol* **32:** 2224–2238. doi:10.1128/MCB.06550-11

Chen Y, Zubovic L, Yang F, Godin K, Pavelitz T, Castellanos J, Macchi P, Varani G. 2016. Rbfox proteins regulate microRNA biogenesis by sequence-specific binding to their precursors and target downstream Dicer. *Nucleic Acids Res* **44:** 4381–4395. doi:10.1093/nar/gkw177

Choi KS, Mizutani A, Lai MM. 2004. SYNCRIP, a member of the heterogeneous nuclear ribonucleoprotein family, is involved in mouse hepatitis virus RNA synthesis. *J Virol* **78:** 13153–13162. doi:10.1128/JVI.78.23.13153-13162.2004

Choudhury NR, de Lima Alves F, de Andres-Aguayo L, Graf T, Caceres JF, Rappsilber J, Michlewski G. 2013. Tissue-specific control of brain-enriched miR-7 biogenesis. *Genes Dev* **27:** 24–38. doi:10.1101/gad.199190.112

Croce CM. 2009. Causes and consequences of microRNA dysregulation in cancer. *Nat Rev Genet* **10:** 704–714. doi:10.1038/nrg2634

Emsley P, Cowtan K. 2004. *Coot*: model-building tools for molecular graphics. *Acta Crystallogr D Biol Crystallogr* **60:** 2126–2132. doi:10.1107/S0907444904019158

Fabian MR, Sonenberg N, Filipowicz W. 2010. Regulation of mRNA translation and stability by microRNAs. *Annu Rev Biochem* **79:** 351–379. doi:10.1146/annurev-biochem-060308-103103

Farh KK, Grimson A, Jan C, Lewis BP, Johnston WK, Lim LP, Burge CB, Bartel DP. 2005. The widespread impact of mammalian microRNAs on mRNA repression and evolution. *Science* **310:** 1817–1821. doi:10.1126/science.1121158

Gebert LFR, MacRae IJ. 2019. Regulation of microRNA function in animals. *Nat Rev Mol Cell Biol* **20:** 21–37. doi:10.1038/s41580-018-0045-7

Guil S, Cáceres JF. 2007. The multifunctional RNA-binding protein hnRNP A1 is required for processing of miR-18a. *Nat Struct Mol Biol* **14:** 591–596. doi:10.1038/nsmb1250

Halstead JM, Lin YQ, Durraine L, Hamilton RS, Ball G, Neely GG, Bellen HJ, Davis I. 2014. Syncrip/hnRNP Q influences synaptic transmission and regulates BMP signaling at the *Drosophila* neuromuscular synapse. *Biol Open* **3:** 839–849. doi:10.1242/bio.20149027

Heo I, Joo C, Cho J, Ha M, Han J, Kim VN. 2008. Lin28 mediates the terminal uridylation of let-7 precursor microRNA. *Mol Cell* **32:** 276–284. doi:10.1016/j.molcel.2008.09.014

Hobor F, Dallmann A, Ball NJ, Cicchini C, Battistelli C, Ogrodowicz RW, Christodoulou E, Martin SR, Castello A, Tripodi M, et al. 2018. A cryptic RNA-binding domain mediates Syncrip recognition and exosomal partitioning of miRNA targets. *Nat Commun* **9:** 831. doi:10.1038/s41467-018-03182-3

Hutvagner G, McLachlan J, Pasquinelli AE, Balint E, Tuschl T, Zamore PD. 2001. A cellular function for the RNA-interference enzyme Dicer in the maturation of the let-7 small temporal RNA. *Science* **293:** 834–838. doi:10.1126/science.1062961

Iioka H, Loiselle D, Haystead TA, Macara IG. 2011. Efficient detection of RNA-protein interactions using tethered RNAs. *Nucleic Acids Res* **39:** e53. doi:10.1093/nar/gkq1316

Kabat JL, Barberan-Soler S, Zahler AM. 2009. HRP-2, the *Caenorhabditis elegans* homolog of mammalian heterogeneous nuclear ribonucleoproteins Q and R, is an alternative splicing factor that binds to UCUAUC splicing regulatory elements. *J Biol Chem* **284:** 28490–28497. doi:10.1074/jbc.M109.023101

Ketting RF, Fischer SE, Bernstein E, Sijen T, Hannon GJ, Plasterk RH. 2001. Dicer functions in RNA interference and in synthesis of small RNA involved in developmental timing in *C. elegans*. *Genes Dev* **15:** 2654–2659. doi:10.1101/gad.927801

Kiledjian M, Dreyfuss G. 1992. Primary structure and binding activity of the hnRNP U protein: binding RNA through RGG box. *EMBO J* **11:** 2655–2664. doi:10.1002/j.1460-2075.1992.tb05331.x

Kim TD, Woo KC, Cho S, Ha DC, Jang SK, Kim KT. 2007. Rhythmic control of AANAT translation by hnRNP Q in circadian melatonin production. *Genes Dev* **21:** 797–810. doi:10.1101/gad.1519507

Kim DY, Woo KC, Lee KH, Kim TD, Kim KT. 2010. hnRNP Q and PTB modulate the circadian oscillation of mouse Rev-erb α via IRES-mediated translation. *Nucleic Acids Res* **38:** 7068–7078. doi:10.1093/nar/gkq569

Kim DY, Kwak E, Kim SH, Lee KH, Woo KC, Kim KT. 2011. hnRNP Q mediates a phase-dependent translation-coupled mRNA decay of mouse *Period3*. *Nucleic Acids Res* **39:** 8901–8914. doi:10.1093/nar/gkr605

Kim DY, Kim W, Lee KH, Kim SH, Lee HR, Kim HJ, Jung Y, Choi JH, Kim KT. 2013. hnRNP Q regulates translation of p53 in normal and stress conditions. *Cell Death Differ* **20:** 226–234. doi:10.1038/cdd.2012.109

Kobayashi H, Tomari Y. 2016. RISC assembly: coordination between small RNAs and Argonaute proteins. *Biochim Biophys Acta* **1859:** 71–81. doi:10.1016/j.bbagrm.2015.08.007

Kooshapur H, Choudhury NR, Simon B, Mühlbauer M, Jussupow A, Fernandez N, Jones AN, Dallmann A, Gabel F, Camilloni C, et al. 2018. Structural basis for terminal loop recognition and stimulation of pri-miRNA-18a processing by hnRNP A1. *Nat Commun* **9:** 2479. doi:10.1038/s41467-018-04871-9

Lee Y, Ahn C, Han J, Choi H, Kim J, Yim J, Lee J, Provost P, Radmark O, Kim S, et al. 2003. The nuclear RNase III Drosha initiates microRNA processing. *Nature* **425:** 415–419. doi:10.1038/nature01957

Lee Y, Kim M, Han J, Yeom KH, Lee S, Baek SH, Kim VN. 2004. MicroRNA genes are transcribed by RNA polymerase II. *EMBO J* **23:** 4051–4060. doi:10.1038/sj.emboj.7600385

Lin SB, Gregory RI. 2015. MicroRNA biogenesis pathways in cancer. *Nat Rev Cancer* **15:** 321–333. doi:10.1038/nrc3932

Liu Q, Lv GD, Qin X, Gen YH, Zheng ST, Liu T, Lu XM. 2012. Role of microRNA let-7 and effect to HMGA2 in esophageal squamous cell carcinoma. *Mol Biol Rep* **39:** 1239–1246. doi:10.1007/s11033-011-0854-7

Lund E, Guttinger S, Calado A, Dahlberg JE, Kutay U. 2004. Nuclear export of microRNA precursors. *Science* **303:** 95–98. doi:10.1126/science.1090599

McDermott SM, Meignin C, Rappsilber J, Davis I. 2012. *Drosophila* Syncrip binds the *gurken* mRNA localisation signal and regulates localised transcripts during axis specification. *Biol Open* **1:** 488–497. doi:10.1242/bio.2012885

McDermott SM, Yang L, Halstead JM, Hamilton RS, Meignin C, Davis I. 2014. *Drosophila* Syncrip modulates the expression of mRNAs encoding key synaptic proteins required for morphology at the neuromuscular junction. *RNA* **20:** 1593–1606. doi:10.1261/rna.045849.114

Mendell JT, Olson EN. 2012. MicroRNAs in stress signaling and human disease. *Cell* **148:** 1172–1187. doi:10.1016/j.cell.2012.02.005

Michlewski G, Cáceres JF. 2010. Antagonistic role of hnRNP A1 and KSRP in the regulation of let-7a biogenesis. *Nat Struct Mol Biol* **17:** 1011–1018. doi:10.1038/nsmb.1874

Michlewski G, Cáceres JF. 2019. Post-transcriptional control of miRNA biogenesis. *RNA* **25:** 1–16. doi:10.1261/rna.068692.118

Navaza J, Saludjian P. 1997. AMoRe: an automated molecular replacement program package. *Methods Enzymol* **276:** 581–594. doi:10.1016/S0076-6879(97)76079-8

Nguyen TA, Jo MH, Choi YG, Park J, Kwon SC, Hohng S, Kim VN, Woo JS. 2015. Functional anatomy of the human microprocessor. *Cell* **161:** 1374–1387. doi:10.1016/j.cell.2015.05.010

Otwinowski Z, Minor W. 1997. Processing of X-ray diffraction data collected in oscillation mode. *Methods Enzymol* **276:** 307–326. doi:10.1016/S0076-6879(97)76066-X

Pekarsky Y, Croce CM. 2015. Role of *miR-15/16* in CLL. *Cell Death Differ* **22:** 6–11. doi:10.1038/cdd.2014.87

Reinhart BJ, Slack FJ, Basson M, Pasquinelli AE, Bettinger JC, Rougvie AE, Horvitz HR, Ruvkun G. 2000. The 21-nucleotide let-7 RNA regulates developmental timing in *Caenorhabditis elegans*. *Nature* **403:** 901–906. doi:10.1038/35002607

Santangelo L, Giurato G, Cicchini C, Montaldo C, Mancone C, Tarallo R, Battistelli C, Alonzi T, Weisz A, Tripodi M. 2016. The RNA-binding protein SYNCRIP is a component of the hepatocyte exosomal machinery controlling microRNA sorting. *Cell Rep* **17:** 799–808. doi:10.1016/j.celrep.2016.09.031

Sokol NS, Xu P, Jan YN, Ambros V. 2008. *Drosophila* let-7 microRNA is required for remodeling of the neuromusculature during metamorphosis. *Genes Dev* **22:** 1591–1596. doi:10.1101/gad.1671708

Svitkin YV, Yanagiya A, Karetnikov AE, Alain T, Fabian MR, Khoutorsky A, Perreault S, Topisirovic I, Sonenberg N. 2013. Control of translation and miRNA-dependent repression by a novel poly(A) binding protein, hnRNP-Q. *PLoS Biol* **11:** e1001564. doi:10.1371/journal.pbio.1001564

Treiber T, Treiber N, Plessmann U, Harlander S, Daiss JL, Eichner N, Lehmann G, Schall K, Urlaub H, Meister G. 2017. A compendium of RNA-binding proteins that regulate microRNA biogenesis. *Mol Cell* **66:** 270–284 e213. doi:10.1016/j.molcel.2017.03.014

Wang F, Song W, Zhao H, Ma Y, Li Y, Zhai D, Pi J, Si Y, Xu J, Dong L, et al. 2017. The RNA-binding protein QKI5 regulates primary miR-124-1 processing via a distal RNA motif during erythropoiesis. *Cell Res* **27:** 416–439. doi:10.1038/cr.2017.26

Williams KR, McAninch DS, Stefanovic S, Xing L, Allen M, Li W, Feng Y, Mihailescu MR, Bassell GJ. 2016. hnRNP-Q1 represses nascent axon growth in cortical neurons by inhibiting *Gap-43* mRNA translation. *Mol Biol Cell* **27:** 518–534. doi:10.1091/mbc.e15-07-0504

Yi R, Qin Y, Macara IG, Cullen BR. 2003. Exportin-5 mediates the nuclear export of pre-microRNAs and short hairpin RNAs. *Genes Dev* **17:** 3011–3016. doi:10.1101/gad.1158803

Zheng Q, Yang HJ, Yuan YA. 2017. Autoantigen La regulates microRNA processing from stem–loop precursors by association with DGCR8. *Biochemistry* **56:** 6098–6110. doi:10.1021/acs.biochem.7b00693